

pubs.acs.org/NanoLett Letter

Dopant Segregation Inside and Outside Dislocation Cores in Perovskite BaSnO₃ and Reconstruction of the Local Atomic and Electronic Structures

Hwanhui Yun,* Abhinav Prakash, Turan Birol, Bharat Jalan, and K. Andre Mkhoyan*



Cite This: Nano Lett. 2021, 21, 4357-4364



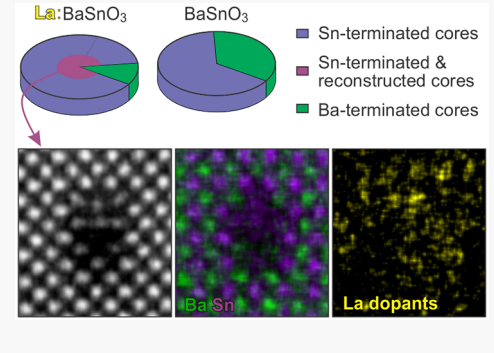
ACCESS

III Metrics & More

Article Recommendations

Supporting Information

ABSTRACT: Distinct dopant behaviors inside and outside dislocation cores are identified by atomic-resolution electron microscopy in perovskite BaSnO₃ with considerable consequences on local atomic and electronic structures. Driven by elastic strain, when A-site designated La dopants segregate near a dislocation core, the dopant atoms accumulate at the Ba sites in compressively strained regions. This triggers formation of Ba vacancies adjacent to the core atomic sites resulting in reconstruction of the core. Notwithstanding the presence of extremely large tensile strain fields, when La atoms segregate inside the dislocation core, they become B-site dopants, replacing Sn atoms and compensating the positive charge of the core oxygen vacancies. Electron energy-loss spectroscopy shows that the local electronic structure of these dislocations changes dramatically due to segregation of the dopants inside and around the core ranging from formation of strong La–O



hybridized electronic states near the conduction band minimum to insulator-to-metal transition.

KEYWORDS: Dislocation, Dopant, Segregation, Core reconstruction, STEM, EELS, EDX

INTRODUCTION

Dislocations, which are topological 1D defects in crystals, are the most common extended defects in crystalline materials and, when present at high concentrations, play a critical role in determining the overall properties of materials ranging from mechanical to electronic. 1,2 In thin films, high density of dislocations can form as misfit dislocations (MDs) at the filmsubstrate interface to accommodate lattice mismatch and as threading dislocations (TDs) propagating along the film growth direction to accommodate local strain or small-angle grain tilts. In-depth characterization of these dislocations and understanding their effects on the properties in perovskite oxide thin films is in high demand as they are linked to the factors limiting novel functionalities of these perovskites.^{3–5} Zhang et al.^{6,7} have identified the basic core atomic structures of the two main TDs in the prototypical perovskite oxide $SrTiO_3$: single ([001]/(100)-type) and dissociated ([001]/ (110)-type) edge dislocations. The core structure of edge dislocation, formed at the edge of an extra half-plane, is susceptible to modifications in these perovskites because the extra half-plane here is a set of atomic planes allowing widerange structural possibilities. In particular, understanding the effects of doping on structural and electronic changes in these edge TDs is of broad interest, which are not well-studied in perovskite oxides even though they have been studied theoretically^{2,8,9} and experimentally in other oxides,¹⁰ nitrides, 11,12 and metals with micro- and nanoscale probes. The lack of understanding of the atomic-level specifics of dislocation-dopant interaction limits both dopant engineering for electronic purposes and dislocation engineering for mechanical purposes.

In this report, we present an atomic-level study of dislocation-dopant interaction in perovskite oxide BaSnO₃ (BSO) thin films using aberration-corrected scanning transmission electron microscopy (STEM) with sub-Å resolution imaging combined with energy dispersive X-ray spectroscopy (EDX) and electron energy-loss spectroscopy (EELS), which is an excellent method for both dopant identification 14-17 and dislocation studies. 6,7,18,19 The selection of BSO for this dislocation-dopant interaction study was based on several favorable factors: 3.0 eV wide band gap with tunability using strain, ^{20,21} excellent thermal stability, and outstanding electron mobility when doped in La, which is also known to be limited due to charged TDs^{22–26} suggesting active interaction between La dopants and TDs. Here, STEM measurements of undoped and La-doped (2%) BSO (LBSO) films grown by hybrid molecular beam epitaxy (MBE) allowed precise identification of the dislocation core structures and dopant atom locations

Received: March 9, 2021 Revised: May 6, 2021 Published: May 11, 2021





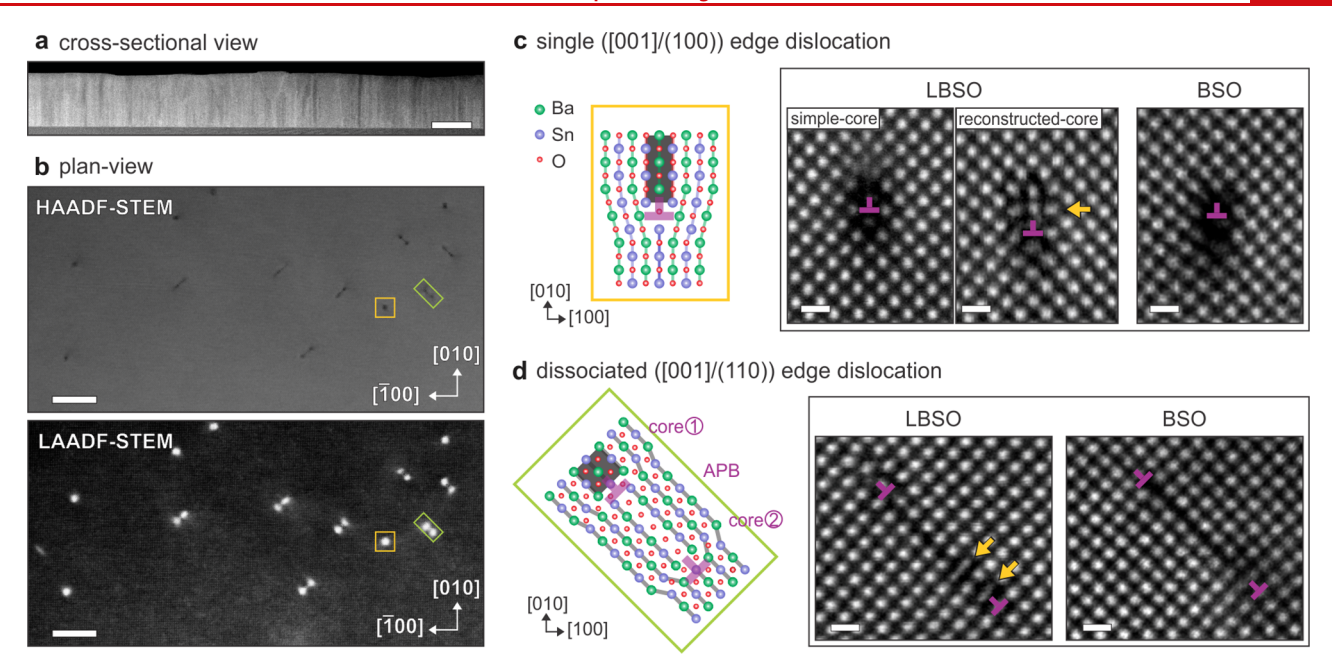


Figure 1. STEM images of edge dislocations in an LBSO thin film. (a) Cross-sectional HAADF-STEM image of an LBSO thin film on a SrTiO $_3$ substrate. Scale bar is 100 nm. (b) Plan-view HAADF- and LAADF-STEM images of an LBSO thin film. A single ([001]/(100)-type) dislocation and a dissociated ([001]/(110)-type) dislocation are highlighted in yellow and green boxes. Scale bars are 10 nm. (c, d) Atomic structures of single (c) and dissociated (d) dislocations. Simplified atomic models are shown on the left where the core is indicated with a dislocation symbol, and extra half atomic planes are indicated by a dark gray shade. HAADF-STEM images acquired from edge dislocations in LBSO and BSO thin films are displayed on the right. Unique structures observed only in LBSO are indicated by yellow arrows. Scale bars are 0.5 nm.

inside and around dislocations using high-angle annular dark-field (HAADF) images and EDX maps. Core-level EELS measurements from oxygen atoms and complementary *ab initio* calculations were also employed linking La dopant effects to the changes in local electronic structure.

■ RESULTS AND DISCUSSION

A cross-sectional HAADF-STEM image of an LBSO thin film grown by a hybrid MBE method on a SrTiO3 substrate is shown in Figure 1(a) (see the Supporting Information (SI), Materials and Methods). Here, vertical line contrasts across the film indicate TDs in the film. The TDs, particularly edge dislocations, are clearly visible in plan-view STEM images (Figure 1(b)). They appear as dark spots in the HAADF image due to the lower density of atomic columns and as strong bright spots in the low-angle annular dark-field (LAADF) image due to the strong strain field around the dislocations. Two common edge dislocations^{6,7} observed in these films are a single dislocation with a Burgers vector $\mathbf{b} = \mathbf{a}_{BSO} \langle 100 \rangle$, which appears as a single spot in the STEM images (yellow box, in Figure 1(b)), and a dissociated dislocation with $\mathbf{b} = \mathbf{a}_{BSO} \langle 110 \rangle$, which appears as paired spots (green box, in Figure 1(b)). In the case of a single dislocation, an extra half-plane is a set of two atomic planes, BaO and SnO2, running along one of the $\langle 100 \rangle$ directions (Figure 1(c)). On the other hand, the extra half-plane in a dissociated dislocation is composed of two BaSnO and two O_2 planes running along one of the $\langle 110 \rangle$ directions. This dislocation is formed from two "dissociated" partial cores connected by a few-unit-cell-long antiphase boundary (APB) (Figure 1(d)).

STEM image analysis, based on more than 200 individual TDs in LBSO and BSO films (SI, Figure S1), indicates that the effects of La dopants on the structure of these edge TDs are quite dramatic. First, in LBSO films, single dislocations with a

unique reconstructed-core structure featured by five atomic columns arranged in a "cross" shape were observed in 18% of single dislocations (Figure 1(c), while they were not observed in undoped BSO films. Second, the fraction of Sn-terminated (referring to the edge composition of the extra half-plane) single dislocations has jumped to 89% in LBSO films from only 65% in undoped BSO films. Additionally, at the APB of dissociated dislocations in LBSO films, unexpected atomic displacements were observed; pairs of the atomic columns from the opposite side of the boundary have moved closer to each other (indicated by arrows in Figure 1(d)). While 46% of dissociated dislocations in LBSO showed such an atomic shift, none was observed in undoped BSO. These aberrant features of TDs observed only in LBSO films implicate that La dopants have considerable impact on the atomic structures of the dislocations and, possibly, on their electronic characteristics.

Single [001]/(100)-Type Edge Dislocation. For in-depth evaluation of the effects of La dopants, chemical composition of more common Sn-terminated single dislocations in LBSO was determined using atomic-resolution EDX elemental mapping (Figure 2(a)). The maps of individual elements identify the location of Ba and Sn atoms at the structure and, more importantly, the atomic sites of La dopants. They revealed that the "cross" structure at the center of the reconstructed-core dislocation is comprised of Sn atomic columns. This reconstructed-core structure appears to be rocksalt phase SnO, similar to TiO observed at dislocation cores in SrTiO₃.²⁷ However, formation of other SnO_x compounds, such as SnO2, cannot be ruled out (SI, Figure S1). This observation reinforces results from STEM image analysis that Sn-rich (Ba-depleted) core structures are favored in the presence of La dopants.

La dopant segregation at the core and in the area around the extra half-plane of the dislocation is clearly visible in EDX

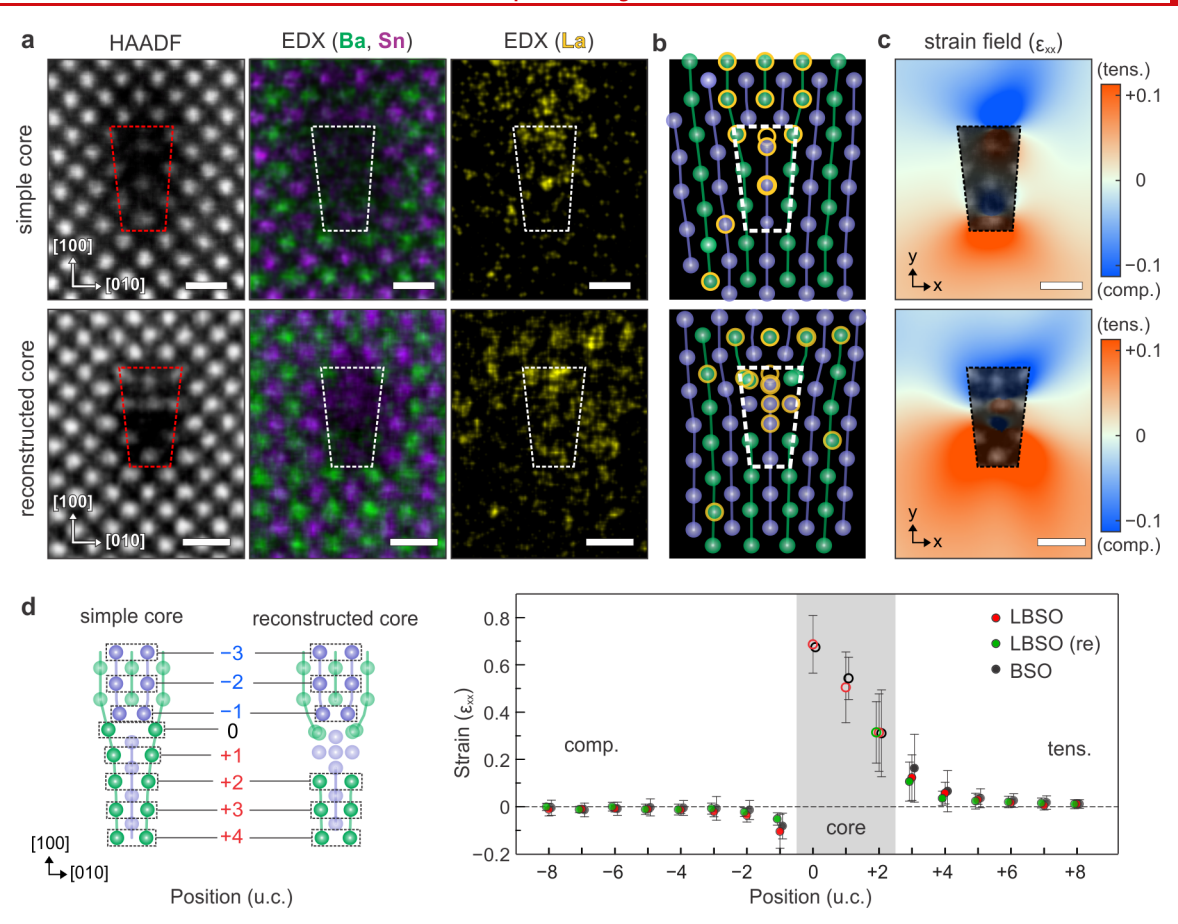


Figure 2. Structural and compositional analyses of single dislocations in LBSO. (a) Atomic-resolution HAADF-STEM images and EDX elemental maps of single dislocations with a simple-core (top) and a reconstructed-core (bottom). The cores are encased by dashed lines. Scale bars are 0.5 nm. Color code of EDX maps: Ba-green, Sn-purple, La-yellow. Ba, Sn, and La maps were acquired using both L_{α} and L_{β} signals. (b) Simplified atomic models of the dislocations illustrating the locations of La atoms (yellow outlines). The color code is the same as in panel (a). (c) Strain field (ε_{xx} , where x is the slip plane direction [010]) maps around the dislocations constructed using GPA. In the core (inside the box with dashed lines), HAADF-STEM images are overlaid. In the core region, GPA analysis is not reliable due to the different atomic configurations from the bulk, and the analysis here is complemented with direct strain evaluation from the interatomic distances. Tensile (+) and compressive (-) strained regions are represented by red and blue colors, respectively. (d) Strain evaluated based on the local lattice constant. The atomic sites utilized to evaluate the local lattice constant are outlined on the schematic on the left. The strains across three single-type dislocations are shown on the right. The core region is indicated by a gray shade.

maps (Figure 2(a,b)). It has markedly different characteristics inside and around the core regardless of the core-type. At the dislocation cores, nominally A-site dopant La atoms are concentrated at Sn sites, which is the B-site, forming antisite defects, La_{Sn}^{1-} . The oxygen vacancies V_{O}^{2+} that are known to form at the dislocation core in perovskite oxides^{6,28-30} are positively charged and, therefore, can attract La dopants and promote formation of the negatively charged La_{Sn} ¹⁻. Outside the core, while being predominantly located at Ba sites (Asite), La atoms distinctly segregate in the compressively strained region near the extra half-plane with the La/Ba ratio up to 0.24 (SI, Figure S2). The strain field maps, constructed from the HAADF-STEM images via geometric phase analysis (GPA)³¹ (Figure 2(c)), show direct correlation between locations of the LaBa 1+ dopants and the zones of the compressive strain around the dislocation. This asymmetric accumulation of ${\rm La_{Ba}}^{1+}$ dopants around the dislocation resembles strain-driven dopant segregation observed in other semiconductors. $^{8,10-12}$ The size of the ${\rm La^{3+}}$ ion is 1.36 Å, which is about 15% smaller than that of the Ba2+ ion (1.61 Å).³² Thus, by occupying Ba sites in the compressive strain zone of the dislocations, La dopants lower the elastic strain

energy. To further confirm that the La dopant segregation around the dislocations in BSO is indeed driven by compressive strain, other extended defects—Ruddlesdenpopper faults and MDs at the BSO-LaAlO₃ interface—in these LBSO films were also investigated. No visible La accumulation was observed around these defects (Figure S3), which is consistent with the absence of compressive strain fields around them. It should be noted that such elastic straindriven accumulation of substitutional dopants around dislocation in oxides has only been computationally predicted but has not been directly demonstrated.

Quantification of the strain fields at these single dislocations (Figure 2(d)), performed using a combination of GPA and interatomic distance analysis methods, showed heavily asymmetric strain distribution across the dislocations with much larger tensile strains in the core due to open spaces there. While outside the core $0.1a_{\rm BSO}$ strains are present in both tensile and compressive sides, at the core, the level of tensile strain is as high as $0.7a_{\rm BSO}$. $a_{\rm BSO}$ is the lattice parameter of BSO. Whereas the change in the lattice parameter due to La substitution in the compressive region, which is expected to be small, less than $0.02a_{\rm BSO}$ (depending on the level of La

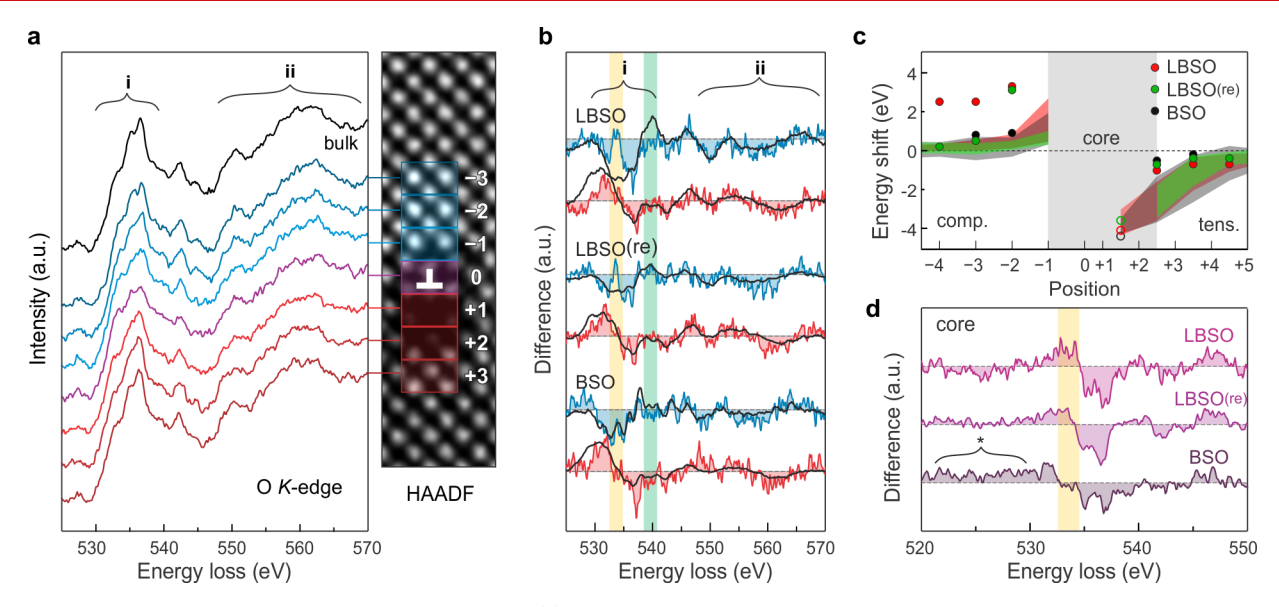


Figure 3. EELS O K edge analysis of single dislocations. (a) O K edge spectra acquired across a reconstructed-core dislocation in LBSO. Acquisition areas are indicated by boxes on the HAADF-STEM image shown on the right with the color of the boxes matching the line colors of the spectra. The reference O K edge obtained from a nearby dislocation-free region (labeled "bulk") is also plotted. The energy windows near the edge onset (i) and the postedge region (ii) are marked. (b) O K edge difference spectra obtained from compressive and tensile zones in three single dislocations—simple-core and reconstructed-core dislocations in LBSO and simple-core dislocation in undoped BSO (colored lines). The fits to the difference spectra due to the energy shift are shown as black lines. The energy windows showing a discrepancy between the experimental and the computed spectra due to $\text{La}_{\text{Ba}}^{-1}$ dopants are highlighted with yellow and green shades. (c) The energy-shift amounts determined from analysis of local O K edges (scatter plots) are compared to the corresponding values from the uniaxial strain-band gap relationship (band plots). (d) O K edge difference spectra from the defect-core (area '0') from all three dislocations. A peak due to the presence of La dopants is indicated by a yellow shade, and the enhanced signal of the Sn $M_{4,5}$ edge accruing only in BSO is highlighted with a brace with an asterisk.

occupancy), cannot be accurately quantified here, strain relaxation around the reconstructed-core dislocations was still detected (Figure 2(d)). Based on these results, it can be predicted that due to higher tensile strains at and around the core of single dislocations, doping with bigger cations than Ba^{2+} or Sn^{4+} can lead to even stronger attraction and heavier accumulation of dopants in BSO films.

The local electronic structures of these single dislocations and the effect of La segregation were probed with core-loss EELS. Here, the O K edge was measured as the fine structure of this edge is highly sensitive to local density of states (DOS) of O 2p orbitals, and these O 2p states are the dominant states in the lower conduction bands of BSO.³³ O K edges with an onset at about 529 eV³⁴ were obtained across both simple-core and reconstructed-core dislocations in LBSO films, as well as across simple-core dislocations in undoped BSO (Figure 3(a) and SI, Figure S4). In the series of O K edges, spectral shape modifications are visible; at the dislocation core, changes appear near the edge onset (i), and outside the core, the changes are in the postedge region (ii). These changes are better visualized in the difference spectra between the local edges and bulk edge (SI, Figure S4).

Our DFT calculations along with recent computational studies 20,21 predict that the band gap of BSO should increase under compressive strain and decrease under tensile strain with no significant changes in DOS of the conduction band (SI, Figure S5). Hence, the changes in O K edges recorded from strain zones outside the core can be evaluated by energy shifts (Figure 3(b)) (for details see SI, Figure S6). In tensile strain zones, which are free of dopants, energy shifts fully describe the changes in the O K edge. In compressive strain zones where La dopants are segregated, there are two notable deviations from pure energy shifts: a rise of a peak at around

534 eV (yellow bands) and a decline of a peak at around 540 eV (green band). Ba substitution with La causes the emergence of La-hybridized O 2p states at around 5 eV above the conduction band minimum (CBM) and loss of Ba-hybridized states at around 11 eV above the CBM, 33 which explains the observed deviations. The energy shifts determined from the difference spectra show blue-shift in the compressive zone and red-shift in the tensile zone confirming predicted band gap changes under strain.^{20,21} However, when compared quantitatively with the energy shift values expected from the strain data across the dislocations (Figure 3(c)), additional blue-shift is noticed in La-concentrated compressive zones in LBSO films. Due to the high density of La in this compressive region, La could be acting more like an alloying element increasing local band gap and inducing considerable electron doping, which, in turn, causes the additional blue-shift in the O K edge. Such blue-shift of core-level spectra associated with local electron doping has been observed in n-doped semiconductors.³⁵ These results also suggest that in BSO it is possible to have band gap closing at and near the dislocation core due to the presence of high tensile strain.

Because the atomic bonding configurations at the dislocation core are different from those in the bulk crystal, the fine structure of the O K edge recorded from the core is expected to be different, particularly at the energies close to the edge onset. Indeed, considerable fine structure changes are observed in EELS O K edges measured from the core of the three single dislocations (Figure 3(d)). While the O K edge spectra (or the difference spectra) from simple-core and reconstructed-core dislocations in LBSO are similar, differences between the O K edges from BSO and LBSO are apparent. One of the major differences is, as before, the appearance of a peak at 534 eV (yellow shade) in LBSO films is due to La-O bonds and O 2p

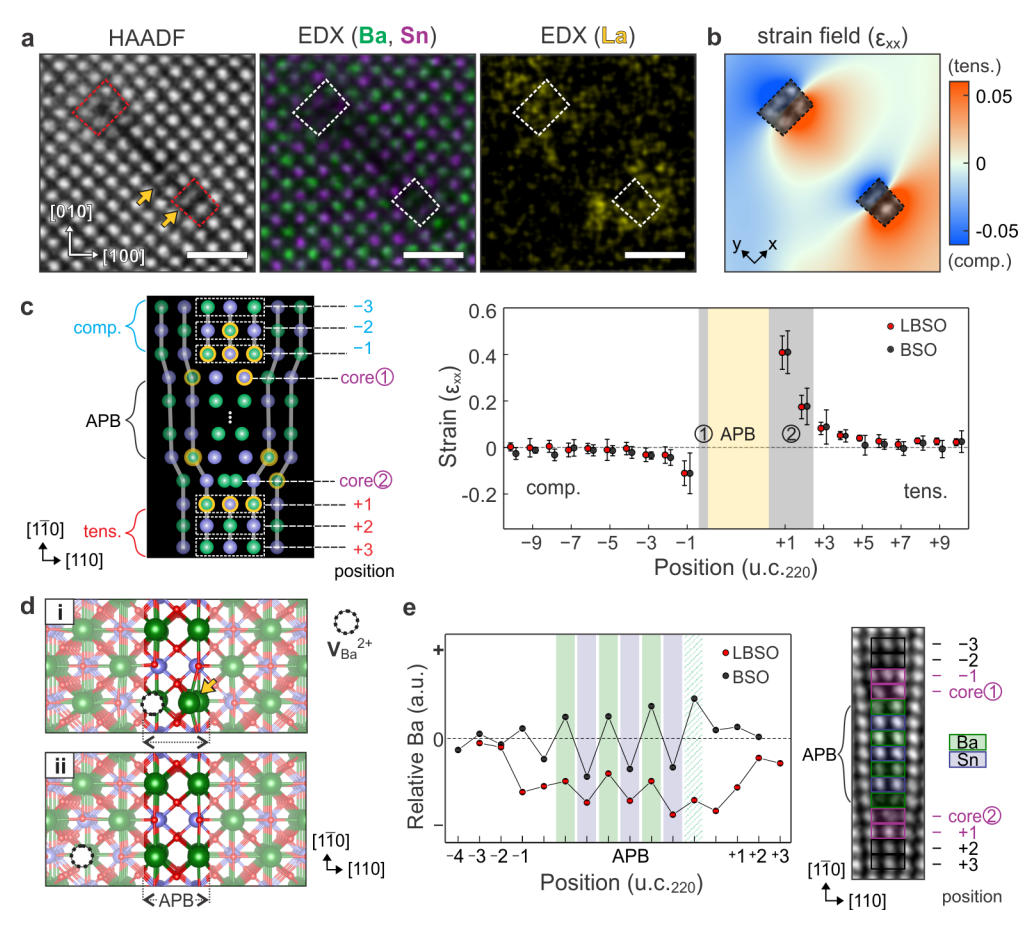


Figure 4. Structural and compositional analyses of dissociated dislocations. (a) HAADF-STEM images and EDX elemental maps of a dissociated dislocation. Two partial cores are indicated by dashed boxes, and displaced Ba atoms at the antiphase-boundary (APB) are indicated by arrows. Scale bars are 1 nm. (b) Strain field (ε_{xxy} where x is the slip plane direction [110]) map around the dislocation constructed using GPA. (c) Strain evaluated from interatomic distances. A simplified atomic model of a dissociated dislocation is shown on the left. La segregation sites are indicated with yellow outlines. Interatomic distances were measured from the atomic sites in the dashed boxes, and the evaluated strain distributions in LBSO and BSO films are presented on the right. (d) Calculated relaxed APB structures with a Ba vacancy at the APB (labeled "i") and outside the APB (labeled "i"). Ba vacancy sites are indicated by dashed open circles, and the Ba atom exhibiting the inward displacement is indicated with an arrow. (e) Relative amount of Ba across a dissociated dislocation evaluated using EELS Ba $M_{4,5}$ edges. Colored boxes on the HAADF-STEM image show the quantification area. In the plot, the positions of Ba and Sn pairs are indicated by green and purple shades, and the one with high Ba deficiency is filled by the dashed shade. The large oscillations of the Ba amount are due to alternating Ba and Sn pairs at the APB.

state hybridization. The second is an increase of the intensity below the 529 eV onset (marked by an asterisk) in undoped BSO. The enhanced signal at these energies is a direct indication of a higher Sn-to-O ratio and red-shift of the Sn $M_{4,5}$ edge due to reduction in the oxidation state of Sn, 38 both of which are consistent with the presence of $V_{\rm O}^{2+}$ in these dislocation cores. Also, ${\rm La_{Sn}}^{1-}$ dopants not only reduce the relative amount of Sn per O but also compensate $V_{\rm O}^{2+}$, thus suppressing an increase of the signal in the Sn $M_{4,5}$ region.

Dissociated [001]/(110)-Type Edge Dislocation. As described earlier, in doped LBSO films, dissociated dislocations show unusual close pairing of some atomic columns at the APB. To determine its correlation with La doping, elemental STEM-EDX analysis was performed (Figure 4(a)). The EDX maps reveal that those uniquely displaced pairs are Ba atomic columns with highly concentrated La columns nearby. Additionally, the strain maps (Figure 4(b)) show that while La segregation at and around two partial cores is similar to those observed in the single dislocations (Figure 2(a,b)), narrow localization of the compressive strain from a lower partial core (core(2)) in the APB region causes heavy La dopant segregation in a few Ba sites available in this region

(Figure 4(a-c)). When the degree of uniaxial strain in the compressive and tensile zones was quantified (Figure 4(c)), it was found that with dissociation of the core the level of tensile strain in these dislocations reduces by about 30-40% relative to those in single dislocations (Figure 2(a,b)), whereas the level of compressive strain stays comparable.

To examine the effect of La dopants on the Ba rearrangement, several DFT-based structure optimizations were performed. First, a supercell containing an APB was constructed and optimized. Then, within this supercell several structural and compositional modifications (including introducing La at different Ba sites) were made and optimized again (SI, Figures S7 and S8). The results show that to induce the inward displacement of Ba atoms at the APB, Ba deficiency is needed at neighboring sites (Figure 4(d)) and that Ba vacancy formation at the APB is energetically favorable compared to others located further from the APB by about 0.8 eV. Therefore, it can be argued that La dopants promote formation of Ba vacancies in nearby Ba sites favorably at the APB, which, in turn, results in a formation of the shifted Ba-Ba pairs bridging the APB. The Ba depletion at the APB due to the presence of La dopants was verified by EELS Ba $M_{4,5}$ analysis

(Figure 4(e) and SI, Figure S9). Local Ba content at the APB in both LBSO and BSO films was evaluated from the intensity of Ba $M_{4,5}$ edges, and the resulting Ba profiles show strong Ba depletion throughout the APB in LBSO films compared to those in undoped BSO. This observation along with analysis of the effects of La dopants on single dislocations discussed earlier highlights a pattern: La segregation around edge dislocations stimulates formation of Ba vacancies, which manifest themselves as prevalence of Sn-terminated cores and formation of the SnO $_x$ phase in single dislocations, and Ba deficiency at the APB in dissociated dislocations. It should be noted that such an increase of Ba vacancies at TDs in LBSO films, which leads to acceptor-like behavior of TDs, was predicted based on electron transport measurements.

The electronic structure of the APB in dissociated dislocations was investigated with core-loss EELS by analyzing O K edges recorded along the APB in LBSO and BSO films (Figure S(a) and SI, Figure S(0)). Also, site-projected O partial

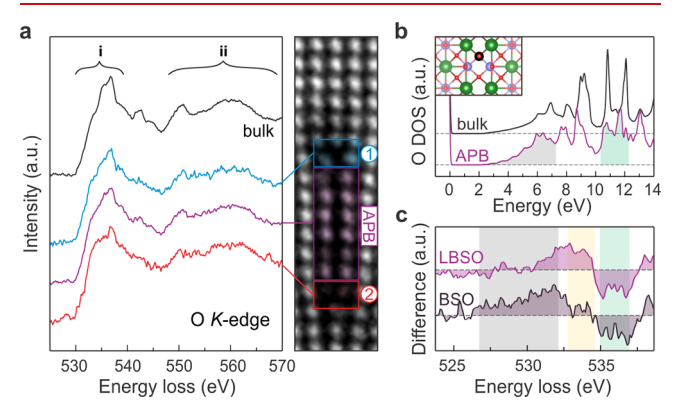


Figure 5. EELS O *K* edge analysis of a dissociated dislocation. (a) O *K* edge spectra acquired across a dissociated dislocation in an LBSO film. The EELS acquisition areas are indicated by boxes with the same color codes as the spectra. (b) Comparison of calculated O 2*p*-DOS at the APB and in the bulk BSO. The site of the oxygen atom at the APB is marked with a circle in the inset atomic model. The electronic states that are responsible for the changes in the O *K* edge fine structure at the APB are indicated by gray and green shades. (c) O *K* edge difference spectra obtained from the APB (averaged over all spectra from the APB) and two cores of dissociated dislocations in both LBSO and undoped BSO films. The energy windows with visible changes due to changes in DOS at the APB are shaded purple and green, and the window with an increased signal due to La-hybridized O states is shaded yellow.

DOS of the conduction band for the oxygen atoms at the APB and in the bulk undoped BSO were calculated for comparison (Figure 5(b) and SI, Figure S11). Based on these calculations, a rise in the DOS near the onset (gray shade) and reduction of states at about 8 eV above the onset (green shade) are expected at the APB sites. Both of these predictions were confirmed by EELS measurements; the O K edge difference spectra from the APB in undoped BSO (Figure 5(c)) showed the increase of the intensity at 528-535 eV (gray shade) and dampening at 535-537 eV (green shade). However, when the same measurements were performed in LBSO films, the results were different; the intensities at about 534 eV are intensified consistent with La hybridization of O 2p states, and notably, intensities near the onset are suppressed suggesting La-driven filling of the first 1–2 eV of CBM due to donation of electrons from La dopants. Therefore, it can be argued that these APBs

of the dissociated dislocations in LBSO films are metallic-like, which is a result of La doping and changes in the local electronic band structures.

Precise identification of the locations of dopant atoms inside and around dislocation cores in La-doped BSO films, achieved using atomic-resolution STEM imaging and elemental mapping, shed light onto the details of dopant-dislocation attraction. STEM-EELS measurements further clarified the consequences of dopant segregation on the electronic properties of the dislocations. For both single and dissociated dislocations, La dopants are largely located at Ba sites (La_{Ba}⁺), thus reducing the stress in the compressively strained regions. However, inside the core, they are located at Sn antisites (La_{Sn}^{-}) to compensate oxygen vacancies (V_{O}^{2+}) . This stark difference is a result of the long-range, strain-driven attraction of dopants around the dislocation, and the shorter-range, Coulombic interaction-driven attraction inside the core. When La dopants segregate around the dislocation core and substitute Ba, they also promote Ba vacancies at the edges of the dislocation core. Consequently, this gives rise to a Snterminated core and formation of a 1-D SnO phase in single dislocations and displacement of Ba atoms at the APB in dissociated dislocations. Analysis of the EELS O K edges shows that La doping also causes changes to the conduction band by the introduction of new La-O hybridized states. The effect of La doping is even more dramatic for dissociated dislocations, where it causes electron accumulation in the lower conduction band at the APB making it metallic. These results show that dopant-based dislocation engineering in perovskite oxides has enormous potential ranging from strain control to dislocationlimited carrier mobility improvements to turning dislocations into metallic lines and much more.

ASSOCIATED CONTENT

Supporting Information

The Supporting Information is available free of charge at https://pubs.acs.org/doi/10.1021/acs.nanolett.1c00966.

Materials and Methods (STEM characterization, strain analysis, DFT calculations), atomic models of edge dislocations in BSO, quantification of La dopants around single TDs using EDX spectra, chemical composition analysis of Ruddlesden–Popper fault and MD at LBSO-LaAlO₃ interface, EELS core-loss O *K* edges from single dislocations, strain effect on electronic structure of BSO computed using DFT, evaluation of energy shift from O *K* edge, APB structure evaluation using DFT calculations, structure optimization of symmetry-broken APB structure, quantification of Ba and La at dissociated dislocation using EELS core-loss O *K* edges collected from dissociated dislocations, and DOS of APB structure in BSO computed using DFT (PDF)

AUTHOR INFORMATION

Corresponding Authors

Hwanhui Yun – Department of Chemical Engineering and Materials Science, University of Minnesota, Minneapolis, Minnesota 55455, United States; Email: yunxx133@ umn.edu

K. Andre Mkhoyan – Department of Chemical Engineering and Materials Science, University of Minnesota, Minneapolis,

Minnesota 55455, United States; o orcid.org/0000-0003-3568-5452; Email: mkhoyan@umn.edu

Authors

- Abhinav Prakash Department of Chemical Engineering and Materials Science, University of Minnesota, Minneapolis, Minnesota 55455, United States; orcid.org/0000-0002-8899-0568
- Turan Birol Department of Chemical Engineering and Materials Science, University of Minnesota, Minneapolis, Minnesota 55455, United States; ⊙ orcid.org/0000-0001-5174-3320
- Bharat Jalan Department of Chemical Engineering and Materials Science, University of Minnesota, Minneapolis, Minnesota 55455, United States; orcid.org/0000-0002-7940-0490

Complete contact information is available at: https://pubs.acs.org/10.1021/acs.nanolett.1c00966

Author Contributions

H.Y. and K.A.M conceived the project. H.Y. performed STEM experiments with input from K.A.M. and *ab initio* calculations with input from K.A.M. and T.B. A.P. grew thin films by hybrid MBE with input from B.J. H.Y. and K.A.M. prepared the manuscript with contributions from all authors. K.A.M. directed all aspects of the project.

Notes

The authors declare no competing financial interest.

ACKNOWLEDGMENTS

This work is supported primarily by the National Science Foundation (NSF) through the UMN MRSEC under Awards DMR-1420013 and DMR-2011401. This work utilized the UMN Characterization Facility, supported in part by the NSF through the UMN MRSEC program. The MBE growth work was supported primarily by the U.S. Department of Energy (DOE) through No. DE-SC0020211. A.P. acknowledges support from the University of Minnesota Doctoral Dissertation Fellowship.

REFERENCES

- (1) Anderson, P. M.; Hirth, J. P.; Lothe, J. *Theory of Dislocations*; Cambridge University Press: Cambridge, 2017.
- (2) Holt, D. B.; Yacobi, B. G. Extended Defects in Semiconductors Electronic Properties, Device Effects and Structures; Cambridge University Press: Cambridge, 2007; DOI: 10.1017/CBO9780511534850.
- (3) Cava, R. J.; et al. Bulk superconductivity at 91 K in single-phase oxygen-deficient perovskite Ba₂YCu₃O_{9-δ}. *Phys. Rev. Lett.* **1987**, 58, 1676–1679.
- (4) Goodenough, J. B. Electronic and ionic transport properties and other physical aspects of perovskites. *Rep. Prog. Phys.* **2004**, *67*, 1915–1993.
- (5) Haeni, J. H.; et al. Room-temperature ferroelectricity in strained SrTiO₃. *Nature* **2004**, *430*, 758–761.
- (6) Zhang, Z.; Sigle, W.; Rühle, M. Atomic and electronic characterization of the a[100] dislocation core in SrTiO₃. *Phys. Rev. B: Condens. Matter Mater. Phys.* **2002**, *66*, 094108.
- (7) Zhang, Z.; Sigle, W.; Kurtz, W.; Rühle, M. Electronic and atomic structure of a dissociated dislocation in SrTiO₃. *Phys. Rev. B: Condens. Matter Mater. Phys.* **2002**, *66*, 214112.
- (8) Sun, L.; Marrocchelli, D.; Yildiz, B. Edge dislocation slows down oxide ion diffusion in doped CeO₂ by segregation of charged defects. *Nat. Commun.* **2015**, *6*, 6294.

- (9) Fiore, N. F.; Bauer, C. L. Binding of solute atoms to dislocations. *Prog. Mater. Sci.* **1968**, *13*, 85–134.
- (10) Roh, J. Y.; Sato, Y.; Ikuhara, Y. Grain Boundary Plane Effect on Pr Segregation Site in ZnO $\sum 13$ [0001] Symmetric Tilt Grain Boundaries. *J. Am. Ceram. Soc.* **2015**, *98*, 1932–1936.
- (11) Rhode, S. K.; et al. Mg doping affects dislocation core structures in GaN. Phys. Rev. Lett. 2013, 111, 025502.
- (12) Horton, M. K.; et al. Segregation of In to Dislocations in InGaN. *Nano Lett.* **2015**, *15*, 923–930.
- (13) Bouchet, D.; Lartigue-Korinek, S.; Molins, R.; Thibault, J. Yttrium segregation and intergranular defects in alumina. *Philos. Mag.* **2006**, *86*, 1401–1413.
- (14) Voyles, P. M.; Muller, D. A.; Grazul, J. L.; Citrin, P. H.; Gossmann, H. J. L. Atomic-scale imaging of individual dopant atoms and clusters in highly n-type bulk Si. *Nature* **2002**, *416*, 826.
- (15) Shibata, N.; et al. Atomic-scale imaging of individual dopant atoms in a buried interface. *Nat. Mater.* **2009**, *8*, 654–658.
- (16) Gunawan, A. A.; Mkhoyan, K. A.; Wills, A. W.; Thomas, M. G.; Norris, D. J. Imaging "invisible" dopant atoms in semiconductor nanocrystals. *Nano Lett.* **2011**, *11*, 5553–5557.
- (17) Hwang, J.; Zhang, J. Y.; D'Alfonso, A. J.; Allen, L. J.; Stemmer, S. Three-dimensional imaging of individual dopant atoms in SrTiO₃. *Phys. Rev. Lett.* **2013**, *111*, 266101.
- (18) Zhang, Z.; Sigle, W.; Phillipp, F.; Rühle, M. Direct atomresolved imaging of oxides and their grain boundaries. *Science* **2003**, 302, 846–849.
- (19) Jia, C. L.; Thust, A.; Urban, K. Atomic-scale analysis of the oxygen configuration at a SrTiO₃ dislocation core. *Phys. Rev. Lett.* **2005**, 95, 225506.
- (20) Singh, D. J.; Xu, Q.; Ong, K. P. Strain effects on the band gap and optical properties of perovskite SrSnO₃ and BaSnO₃. *Appl. Phys. Lett.* **2014**, *104*, 011910.
- (21) Wang, Y.; Sui, R.; Bi, M.; Tang, W.; Ma, S. Strain sensitivity of band structure and electron mobility in perovskite BaSnO₃: first-principles calculation. *RSC Adv.* **2019**, *9*, 14072–14077.
- (22) Kim, H. J.; et al. High mobility in a stable transparent perovskite oxide. *Appl. Phys. Express* **2012**, *5*, 061102.
- (23) Kim, H. J.; et al. Physical properties of transparent perovskite oxides (Ba,La)SnO₃ with high electrical mobility at room temperature. *Phys. Rev. B: Condens. Matter Mater. Phys.* **2012**, *86*, 165205.
- (24) Raghavan, S.; et al. High-mobility BaSnO₃ grown by oxide molecular beam epitaxy. *APL Mater.* **2016**, *4*, 016106.
- (25) Prakash, A.; et al. Wide bandgap BaSnO₃ films with room temperature conductivity exceeding 10⁴ S cm⁻¹. *Nat. Commun.* **2017**, 8, 15167.
- (26) Kim, U.; et al. Dopant-site-dependent scattering by dislocations in epitaxial films of perovskite semiconductor BaSnO₃. *APL Mater.* **2014**, 2, 056107.
- (27) Gao, P.; et al. Atomic-scale structure relaxation, chemistry and charge distribution of dislocation cores in SrTiO₃. *Ultramicroscopy* **2018**, *184*, 217–224.
- (28) Lubk, A.; et al. Electromechanical coupling among edge dislocations, domain walls, and nanodomains in BiFeO $_3$ revealed by unit-cell-wise strain and polarization maps. *Nano Lett.* **2013**, *13*, 1410–1415.
- (29) Marrocchelli, D.; Sun, L.; Yildiz, B. Dislocations in SrTiO₃: Easy to reduce but not so fast for oxygen transport. *J. Am. Chem. Soc.* **2015**, *137*, 4735–4748.
- (30) Hirel, P.; Carrez, P.; Clouet, E.; Cordier, P. The electric charge and climb of edge dislocations in perovskite oxides: The case of high-pressure MgSiO₃ bridgmanite. *Acta Mater.* **2016**, *106*, 313–321.
- (31) Hÿtch, M. J.; Snoeck, E.; Kilaas, R. Quantitative measurement of displacement and strain fields from HREM micrographs. *Ultramicroscopy* **1998**, *74*, 131–146.
- (32) Shannon, R. D. Revised effective ionic radii and systematic studies of interatomic distances in halids and chalcogenides. *Acta Cryst. A* **1976**, *32*, 751.

- (33) Li, Y.; Zhang, L.; Ma, Y.; Singh, D. J. Tuning optical properties of transparent conducting barium stannate by dimensional reduction. *APL Mater.* **2015**, *3*, 011102.
- (34) Yun, H.; et al. Electronic structure of BaSnO₃ investigated by high-energy-resolution electron energy-loss spectroscopy and ab initio calculations. *J. Vac. Sci. Technol., A* **2018**, *36*, 031503.
- (35) Asokan, K.; et al. Electron- and hole-doping effects on the electronic structure of Manganite studied by x-ray absorption spectroscopy. *J. Phys.: Condens. Matter* **2004**, *16*, 3791–3799.
- (36) Sezen, H.; Suzer, S. Communication: Enhancement of dopant dependent x-ray photoelectron spectroscopy peak shifts of Si by surface photovoltage. *J. Chem. Phys.* **2011**, *135*, 141102.
- (37) Horio, M.; et al. Electronic structure of Ce-doped and -undoped Nd₂CuO₄ superconducting thin films studied by hard X-ray photoemission and soft X-ray absorption spectroscopy. *Phys. Rev. Lett.* **2018**, *120*, 257001.
- (38) Egerton, R. F. Electron Energy Loss Spectroscopy in the Electron Microscope, 3rd ed.; Springer: Boston, 2011; DOI: 10.1007/978-1-4419-9583-4.